Available online at www.sciencedirect.com
SCIENCE DIRECT®
ELSEVIER
International Journal of Solids and Structures 43 (2006) 4648–4672
INTERNATIONAL JOURNAL OF SOLIDS and STRUCTURES
www.elsevier.com/locate/ijsolstr

Perturbation methods for the analysis of the dynamic behavior of damaged plates

V.K. Sharma [a], M. Ruzzene [b,*], S. Hanagud [b]

[a] *Millennium Dynamics Corp., Acworth, GA 30101, USA*
[b] *School of Aerospace Engineering, Georgia Institute of Technology, 270 Ferst Drive, Atlanta, GA, 30332-0150, USA*

Received 18 March 2005; received in revised form 7 July 2005
Available online 23 September 2005

Abstract

This paper presents an analytical method for the analysis of the dynamic behavior of damaged plates. The proposed approach allows the derivation of mode shapes and corresponding curvature modes for plates with various kinds of defects. Damage is modeled as a localized reduction in the plate thickness. Both point and line defects are considered to model notches or line cracks and delaminations in the plate. Small thickness reductions are considered so that the dynamic behavior of the damage plate can be analyzed through perturbations with respect to the undamaged modes. Results are presented to demonstrate the sensitivity of the curvature modes with respect to the considered low damage levels. Also, the curvature modes are used for the estimation of the strain energy of the plate and for the formulation of a damage index which can be used to provide damage location and extent information.

Keywords: Perturbation methods; Strain energy ratio; Damaged plates; Curvature modes

1. Introduction

The objective of a structural health monitoring system is to identify anomalies or damages such as cracks, delamination and disbonds in structures. The term identification includes the determination of the existence of damages, their location and their sizes or magnitudes as accurately as possible. This goal can be achieved with the help of analytical formulations for simple structures, which can provide invaluable insight in the interpretation and analysis of the measured dynamic response of structures under investigation.

* Corresponding author. Tel.: +1 404 894 3078; fax: +1 404 894 2760.
E-mail address: massimo.ruzzene@ae.gatech.edu (M. Ruzzene).

0020-7683/$ - see front matter
doi:10.1016/j.ijsolstr.2005.07.053

The effects of cracks on the dynamic behavior of beams and shafts have been studied by many authors. Excellent overviews of the state-of-the-art can be found for example in Staszewski et al. (2004) and Doebling et al. (1996). The analytical modeling of simple beam structures with through-the-width cracks has also engaged many researchers. Most of the existing formulations are based on the description of damage as an equivalent stiffness at the location of the defect. The dynamic behavior of single-sided cracked beams can for example be found in Gudmundson (1984), Ostachowicz and Krawczuk (1990), Krawczuk (2002a); Krawczuk and Ostachowicz (2002) and Krawczuk and Ostachowicz (1995), while the work of Hellan (1984), Atluri (1986) and Haisty and Springer (1988) analyzed the effect of double-sided cracks of equal depth. A different approach of modeling cracked beams consists in using approximated numerical solutions. For example in Christides and Barr (1984), the variation of the fundamental frequency of a simply supported beam with a mid-span crack is evaluated using a two-term Rayleigh–Ritz solution. In the approximation an exponentially decaying crack function was used to simulate damage, and the decay rate of the function was estimated from experimental results. The Galerkin approximation is used alternatively in Shen and Pierre (1990) in order to achieve fast convergence rates, while in Qian et al. (1991), a Finite Element model is used to predict the behavior of a beam with an edge crack. Finally, Luo and Hanagud (1998) and subsequently Lestari (2001) presented a perturbation method to describe the dynamic behavior and in particular the curvature modes of cracked beams. In these works, the perturbation analysis is based on the assumption of a small crack whose depth is defined by a perturbation parameter. The modal behavior of the cracked beams is evaluated through perturbation of the modal parameters of the undamaged beams, so that approximate analytical expressions for the damaged modes can be obtained. The present paper extends the formulation presented in Luo and Hanagud (1998) and Lestari (2001) to plates with localized defects. Both point defects, or notches, as well as line defects are considered to evaluate their effects on natural frequencies, mode shapes and curvatures. Relatively little work can be found in the literature on the analytical modeling of damaged plates. Among the work considered as reference for this study, the contributions by Ostachowicz, Krawczuk and co-workers are here mentioned as relevant to the present investigations (Azak et al., 2001; Krawczuk, 2002b; Krawczuk et al., 2004).

The analytical formulations presented below can be used in support of experimental tests, to analyze data and to supplement the experiments with mechanics-based analysis tools that quantify damage. In particular, the application of scanning laser vibrometry for the detection of dynamic deflection shapes allows unprecedented amounts of information which can be successively used for the evaluation of curvature shapes. The results presented in this work and in Luo and Hanagud (1998) and Lestari (2001), in fact indicate how curvatures are extremely sensitive to damage, and how they can be successfully utilized as part of a damage detection technique.

The paper is organized as follows. The brief introduction given in this section is followed by the presentation of the analytical formulation and of the perturbation analysis for damaged plates given in Section 2. Section 3 then presents results for plates with point defects or notches and discusses the influence of defect size and location on various modal parameters. Section 4 extends the investigation to line defects of various orientation, size and location, while Section 5 presents initial experimental investigations on damaged plates. Finally, Section 6 summarizes the main results of the work and outlines the directions of future research activities.

2. Dynamics of damaged plates

2.1. Equation of motion

The free dynamic behavior of damaged plates can be described by expressions formulated from the general equation of motion for plates of variable thickness, as found in Leissa (1993):

$$\nabla^2(D\nabla^2 w) - (1-\nu)\left(\frac{\partial^2 D}{\partial y^2}\frac{\partial^2 w}{\partial x^2} - 2\frac{\partial^2 D}{\partial y \partial x}\frac{\partial^2 w}{\partial y \partial x} + \frac{\partial^2 D}{\partial x^2}\frac{\partial^2 w}{\partial y^2}\right) + m\frac{\partial^2 w}{\partial t^2} = 0 \tag{1}$$

where $w = w(x,y)$ is the out-of-plane displacement of the plate, $h = h(x,y)$ is the plate thickness, $D = D(x,y) = Eh^3/12(1-\nu^2)$ is the plate rigidity, and $m = m(x,y) = \rho h(x,y)$ is the mass per unit area of the plate. Also E, ρ and ν are the Young's modulus, the density and the Poisson's ratio of the plate material.

2.2. Modeling of notch and line defects

We consider defects described as localized reductions in the plate thickness. Notch-type damage, and line defects along the x and y directions are specifically analyzed according to the configurations presented schematically in Figs. 1 and 2. The line defects can be considered as simplified descriptions of a linear crack or of plate delaminations oriented along the reference axis. The extension of the present formulation to line defects of general orientation does not present any theoretical difficulties. However its implementation and analytical derivations are quite involved, and are not reported in this paper as they do not add significant contributions to the discussion.

Damage is described by expressing the plate thickness at the defect location as

$$h_d = h_0 - h_D \tag{2}$$

where h_0 is the thickness of the undamaged plate and h_D is the thickness of the plate at the damage location. Accordingly, the plate rigidity at the defect site can be expressed as:

$$D_d = \frac{Eh_d^3}{12(1-\nu^2)} = D_0\left(1 - \frac{h_D}{h_0}\right)^3 \tag{3}$$

where $D_0 = Eh_0^3/12(1-\nu^2)$ is the rigidity of the undamaged plate. For a small damage, i.e. for $h_D << h_0$, Eq. (3) can be approximated as:

$$D_d \simeq D_0\left(1 - 3\frac{h_D}{h_0}\right) = D_0(1-\epsilon) \tag{4}$$

where $\epsilon = 3h_D/h_0$. Similarly, the mass per unit area of the plate at the defect site can be expressed as:

$$m_d = m_0\left(1 - \frac{h_D}{h_0}\right) = m_0\left(1 - \frac{1}{3}\epsilon\right) \tag{5}$$

where $m_0 = \rho h_0$ is the mass per unit area of the undamaged plate.

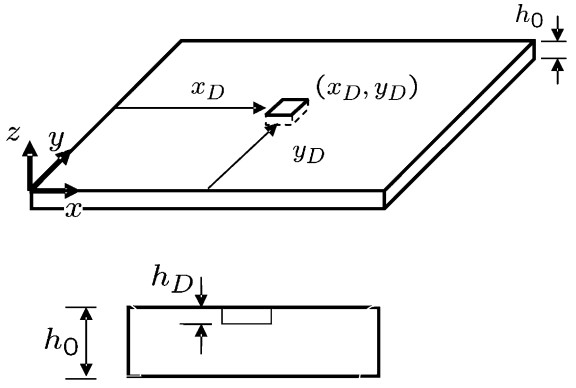

Fig. 1. Schematic of plate with notch damage.

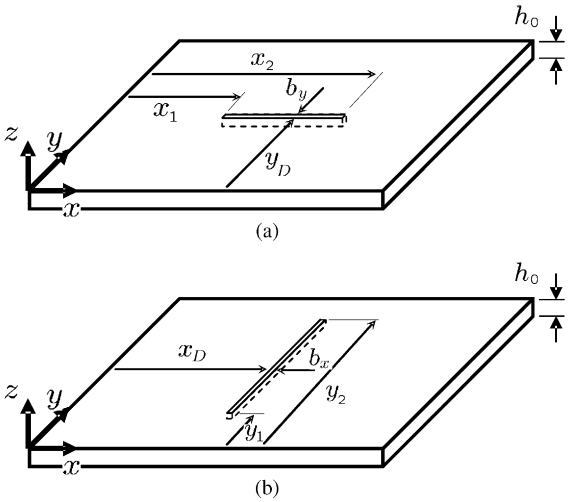

Fig. 2. Schematic of plates with considered line defects.

The plate rigidity $D(x,y)$ can in general be described as:

$$D(x,y) = D_0[1 - \epsilon(H(x-x_1) - H(x-x_2))(H(y-y_1) - H(y-y_2))] \tag{6}$$

where x_1, x_2 and y_1, y_2 define the dimensions of the defect in the x, y directions, and where H is the Heaviside step function. Eq. (6) can be conveniently manipulated to describe both notch-type defects, as well as line loads of the kind shown in Fig. 2. Eq. (6) can in fact be rewritten as:

$$D(x,y) = D_0\left[1 - \epsilon A_{\mathrm{D}} \frac{(H(x-x_1) - H(x-x_2))}{\Delta l_x} \frac{(H(y-y_1) - H(y-y_2))}{\Delta l_y}\right] \tag{7}$$

where $b_x = x_2 - x_1$, $b_y = y_2 - y_1$, and $A_{\mathrm{D}} = b_x * b_y$. For a notch defect at x_{D}, y_{D} (see Fig. 1), it is assumed that

$$x_1 \approx x_2 \approx x_{\mathrm{D}}, \quad y_1 \approx y_2 \approx y_{\mathrm{D}}$$

and Eq. (6) becomes:

$$D(x,y) = D_0[1 - \epsilon A_{\mathrm{D}} \delta(x - x_{\mathrm{D}})\delta(y - y_{\mathrm{D}})] \tag{8}$$

where

$$\delta(x) = \frac{\mathrm{d}H(x)}{\mathrm{d}x}$$

is the Dirac delta function. Similar expressions can be defined to characterize a line defect. For example, a line defect at location $y = y_{\mathrm{D}}$ and parallel to the x direction (Fig. 2a) can be described as:

$$D(x,y) = D_0\left[1 - \epsilon b_y \delta(y - y_{\mathrm{D}}) \int_{x_1}^{x_2} \delta(x - \xi)\,\mathrm{d}\xi\right] \tag{9}$$

while a defect at $x = x_{\mathrm{D}}$ along the y direction (Fig. 2b) can be expressed as:

$$D(x,y) = D_0\left[1 - \epsilon b_x \delta(x - x_D)\int_{y_1}^{y_2} \delta(y-\eta)\,d\eta\right] \tag{10}$$

where x_1, x_2 and y_1, y_2 define the length of the defect, while ξ, η are dummy integration variables. It is worth observing how in Eqs. (9) and (10) the heaviside function is replaced by the integral of the delta function over the extension of the defect. This substitution is adopted in order to take advantage of properties of the delta function which are very convenient for the the analytical derivations presented below.

A general description of line and notch defects of the kind here considered can be obtained by expressing the plate bending rigidity as:

$$D(x,y) = D_0[1 - \epsilon\gamma_D(x,y)] \tag{11}$$

where $\gamma_D(x,y)$ denotes the function describing the considered damage configuration, which can be particularized to the expressions in Eqs. (8)–(10). Similarly, the mass per unit area of the damaged plate can be described as:

$$m(x,y) = m_0\left(1 - \frac{h_d}{h_0}\right) = m_0\left[1 - \frac{1}{3}\epsilon\gamma_D(x,y)\right] \tag{12}$$

The expressions for the plate rigidity and mass given in Eqs. (11) and (12) can be substituted in Eq. (1) to obtain a solution predicting the dynamic behavior of plates with the considered types of damage.

2.3. Perturbation solution

A solution for equation Eq. (1) can be obtained through modal superposition by imposing a solution of the kind:

$$w(x,y) = \sum_{i,j} \phi_{i,j}(x,y)e^{i\omega_{i,j}t} \tag{13}$$

where $\phi_{i,j}$, $\omega_{i,j}$ are respectively the i,jth mode shape and natural frequency (eigensolutions) of the plate, while i is the imaginary unit. Considering for simplicity the contributions of a single mode i,j and substituting Eq. (13) in Eq. (1) gives:

$$\nabla^2\left(D\nabla^2\phi\right) - (1-\nu)\left(\frac{\partial^2 D}{\partial y^2}\frac{\partial^2\phi}{\partial x^2} - 2\frac{\partial^2 D}{\partial y\partial x}\frac{\partial^2\phi}{\partial y\partial x} + \frac{\partial^2 D}{\partial x^2}\frac{\partial^2\phi}{\partial y^2}\right) - m\lambda\phi = 0 \tag{14}$$

where $\lambda = \omega^2$, and where the subscripts i,j are omitted for simplicity. In our analysis, ϵ is assumed to be a small parameter corresponding to a small damage depth h_D. Within this assumption, the eigensolutions for the damaged plate can be expressed as perturbations from the solution for the intact plate, so that the eigenfunctions and eigenvalues of the damaged plate can respectively be expressed as (Luo and Hanagud, 1998):

$$\phi(x,y) = \phi^{(0)}(x,y) - \epsilon\phi^{(1)}(x,y) + \mathcal{O}(\epsilon^2) \tag{15}$$

and

$$\lambda = \lambda^{(0)} - \epsilon\lambda^{(1)} + \mathcal{O}(\epsilon^2) \tag{16}$$

where $\phi^{(0)}(x,y)$, $\lambda^{(0)}$ are the eigensolutions for the undamaged plate, while $\phi^{(1)}(x,y)$, $\lambda^{(1)}$ are the first order perturbations. Substituting the perturbed eigensolutions into Eq. (14), and collecting the coefficients of same power of ϵ gives a set of equations which can be solved in terms of the perturbations coefficients:

$$\epsilon^0: \quad \nabla^4\phi^{(0)} - \frac{m_0}{D_0}\lambda^{(0)}\phi^{(0)} = 0 \tag{17}$$

$$\epsilon^1: \quad \nabla^4\phi^{(1)} + \nabla^2\left[\gamma_D(\phi^{(1)}_{,xx} + \phi^{(1)}_{,yy})\right] = (1-\nu)\left[\phi^{(0)}_{,xx}\gamma_{D,yy} + \phi^{(0)}_{,yy}\gamma_{D,xx} - 2\phi^{(0)}_{,xy}\gamma_{D,xy}\right] + \frac{m_0}{D_0}\left(\lambda^{(0)}\phi^{(1)} + \lambda^{(1)}\phi^{(0)} + \frac{1}{3}\lambda^{(0)}\phi^{(0)}\gamma_D\right) \tag{18}$$

where $\gamma_D = \gamma_D(x,y)$, and where $(\cdot)_{,\zeta}$ denotes partial derivatives with respect to the variable ζ. Eq. (17) represents the equation of motion for an undamaged plate, and its solution provides the undamaged modes $\phi^{(0)}(x,y)$ and eigenvalues $\lambda^{(0)}$, which can then be substituted in Eq. (18) to obtain a solution in terms of the perturbation modal parameters $\phi^{(1)}(x,y)$, $\lambda^{(1)}$.

2.4. Solution of perturbation equations using Fourier series

The i,jth eigenfunction and eigenvalue for a plate supported on all edges are respectively given by (Leissa, 1993):

$$\phi^{(0)}_{i,j}(x,y) = \sin\frac{i\pi x}{L_x}\sin\frac{j\pi y}{L_y} \tag{19}$$

and

$$\lambda^{(0)}_{i,j} = \frac{D_0}{m_0}\left[\left(\frac{i\pi}{L_x}\right)^2 + \left(\frac{j\pi}{L_y}\right)^2\right]^2 \tag{20}$$

where L_x, L_y denote the plate dimensions. An approximate solution for Eq. (18) can be found by imposing a solution of the kind:

$$\phi^{(1)}_{i,j}(x,y) = \sum_p\sum_q \eta_{p,q}\sin\frac{p\pi x}{L_x}\sin\frac{q\pi y}{L_y} \tag{21}$$

which corresponds to the Fourier series expansion of the perturbed mode. Substituting this expansion in Eq. (18) gives:

$$\sum_p\sum_q\left[\left(\left(\frac{p\pi}{L_x}\right)^2 + \left(\frac{q\pi}{L_y}\right)^2\right)^2 - m_0\lambda_0\right]\eta_{p,q}\sin\frac{p\pi x}{L_x}\sin\frac{q\pi y}{L_y} = -(\phi^{(0)}_{,xx} + \phi^{(0)}_{,yy})\nabla^2\gamma_D + (1-\nu)\left[\phi^{(0)}_{,xx}\gamma_{D,yy} + \phi^{(0)}_{,yy}\gamma_{D,xx} - 2\phi^{(0)}_{,xy}\gamma_{D,xy}\right] + \frac{m_0}{D_0}(\lambda^{(1)} + \frac{1}{3}\lambda^{(0)}\gamma_D)\phi^{(0)} \tag{22}$$

where $\phi^{(0)} = \phi^{(0)}_{i,j}(x,y), \lambda^{(0)} = \lambda^{(0)}_{i,j}$ are respectively defined in Eqs. (19) and (20). The complexity of Eq. (22) can be substantially reduced by exploiting the orthogonality properties of harmonic functions. Multiplying Eq. (22) by $\sin\frac{r\pi x}{L_x}\sin\frac{s\pi y}{L_y}$ and integrating over the plate surface gives:

$$\left[\left(\left(\frac{r\pi}{L_x}\right)^2 + \left(\frac{s\pi}{L_y}\right)^2\right)^2 - \left(\left(\frac{i\pi}{L_x}\right)^2 + \left(\frac{j\pi}{L_y}\right)^2\right)^2\right]\eta_{r,s}\frac{L_xL_y}{4} = -\kappa_1 + (1-\nu)\kappa_2 + \frac{m_0}{D_0}\lambda^{(1)}\delta_{ri}\delta_{sj}\frac{L_xL_y}{4} \tag{23}$$

where

$$\kappa_1 = \int_0^{L_x}\int_0^{L_y}\left(\left[\left(\frac{i\pi}{L_x}\right)^2 + \left(\frac{j\pi}{L_y}\right)^2\right]\nabla^2\gamma_D - \frac{1}{3}\frac{m_0}{D_0}\lambda^{(0)}\gamma_D\right)\sin\frac{i\pi x}{L_x}\sin\frac{j\pi y}{L_y}\sin\frac{r\pi x}{L_x}\sin\frac{s\pi y}{L_y}\,dx\,dy$$

and

$$\kappa_2 = \int_0^{L_x}\int_0^{L_y} \phi^{(0)}_{,xx} \sin\frac{r\pi x_D}{L_x}\sin\frac{s\pi y_D}{L_y}\gamma_{D,yy}\,dx\,dy + \int_0^{L_x}\int_0^{L_y} \phi^{(0)}_{,yy} \sin\frac{r\pi x_D}{L_x}\sin\frac{s\pi y_D}{L_y}\gamma_{D,xx}\,dx\,dy - 2\int_0^{L_x}\int_0^{L_y} \phi^{(0)}_{,xx} \sin\frac{r\pi x_D}{L_x}\sin\frac{s\pi y_D}{L_y}\gamma_{D,xy}\,dx\,dy$$

Also, in Eq. (22), $\delta_{k,l}$ is the Kronecker symbol defined as:

$$\delta_{k,l} = \begin{cases} 1 & k = l \\ 0 & k \neq l \end{cases}$$

The summation signs in Eq. (22) are eliminated in virtue of the well-known orthogonality property of harmonic functions, which reads:

$$\int_0^{L_x}\int_0^{L_y} \sin\frac{p\pi x}{L_x}\sin\frac{q\pi y}{L_y}\sin\frac{r\pi x}{L_x}\sin\frac{s\pi y}{L_y}\,dx\,dy = \frac{L_x L_y}{4}\delta_{r,p}\delta_{s,q}$$

and corresponding versions for cosine functions.

Given the considered modes for the undamaged plate, Eq. (23) can be solved in terms of the unknowns $\eta_{r,s}$, $\lambda^{(1)}$. Letting $r = i$ and $s = j$, yields an equation which can be solved in terms of $\lambda^{(1)}_{i,j}$:

$$\lambda^{(1)}_{i,j} = \frac{4D_0}{m_0 L_x L_y}[\kappa_1 - (1-\nu)\kappa_2] \tag{24}$$

It is worth observing how the integrations required for the evaluation of the constants κ_1, κ_2 are significantly simplified by taking advantage of the following properties of the delta function (Jones, 1982):

$$f(x)\delta(x - x_0) = f(x_0)\delta(x) \tag{25}$$

Table 1
Natural frequencies (rad/s) of plates with notch damage

Mode (i,j)	$h_D/h_0 = 0$	$h_D/h_0 = 1\%$	$h_D/h_0 = 2\%$	$h_D/h_0 = 3\%$	$h_D/h_0 = 4\%$
		$x_D = L_x/2$	$y_D = L_y/2$		
1,1	110.6	110.6	110.4	110.2	109.9
1,2	340.3	340.2	339.6	338.8	337.5
2,1	212.7	212.5	212.0	211.1	209.9
2,2	442.5	442.5	442.5	442.5	442.5
1,3	723.2	722.5	720.1	716.2	710.7
		$x_D = L_x/3$	$y_D = L_y/3$		
1,1	110.6	110.5	110.4	110.0	109.6
1,2	340.3	340.1	339.3	338.0	336.1
2,1	212.7	212.6	212.3	211.7	210.9
2,2	442.5	442.2	441.4	440.2	438.4
1,3	723.2	723.0	722.3	721.2	719.5
		$x_D = L_x/5$	$y_D = L_y/5$		
1,1	110.6	110.6	110.4	110.1	109.6
1,2	340.3	340.1	339.4	338.3	336.7
2,1	212.7	212.6	212.1	211.4	210.4
2,2	442.5	442.2	441.6	440.5	439.0
1,3	723.2	722.8	721.3	718.9	715.5

and

$$\int f(x)\frac{\partial^n \delta(x)}{\partial x^n}\mathrm{d}x = \int \frac{\partial f(x)}{\partial x}\frac{\partial^{n-1}\delta(x)}{\partial x^{n-1}}\mathrm{d}x \tag{26}$$

where $f(x)$ is a generic function. A few simple manipulations yield the following expressions:

$$\kappa_1 = \frac{4D_0\Delta A_{\mathrm{D}}}{L_xL_y}\left(\left[\left(\frac{i\pi}{L_x}\right)^2+\left(\frac{j\pi}{L_y}\right)^2\right]-\frac{1}{3}\frac{m_0}{D_0}\lambda^{(0)}\right)\left(\sin\frac{j\pi y_{\mathrm{D}}}{L_y}\right)^2\left(\sin\frac{i\pi x_{\mathrm{D}}}{L_x}\right)^2$$

$$\kappa_1 = \frac{4D_0b_y}{L_xL_y}\left(\left[\left(\frac{i\pi}{L_x}\right)^2+\left(\frac{j\pi}{L_y}\right)^2\right]-\frac{1}{3}\frac{m_0}{D_0}\lambda^{(0)}\right)\left(\sin\frac{j\pi y_{\mathrm{D}}}{L_y}\right)^2\int_{x_1}^{x_2}\left(\sin\frac{i\pi\xi}{L_x}\right)^2\mathrm{d}\xi$$

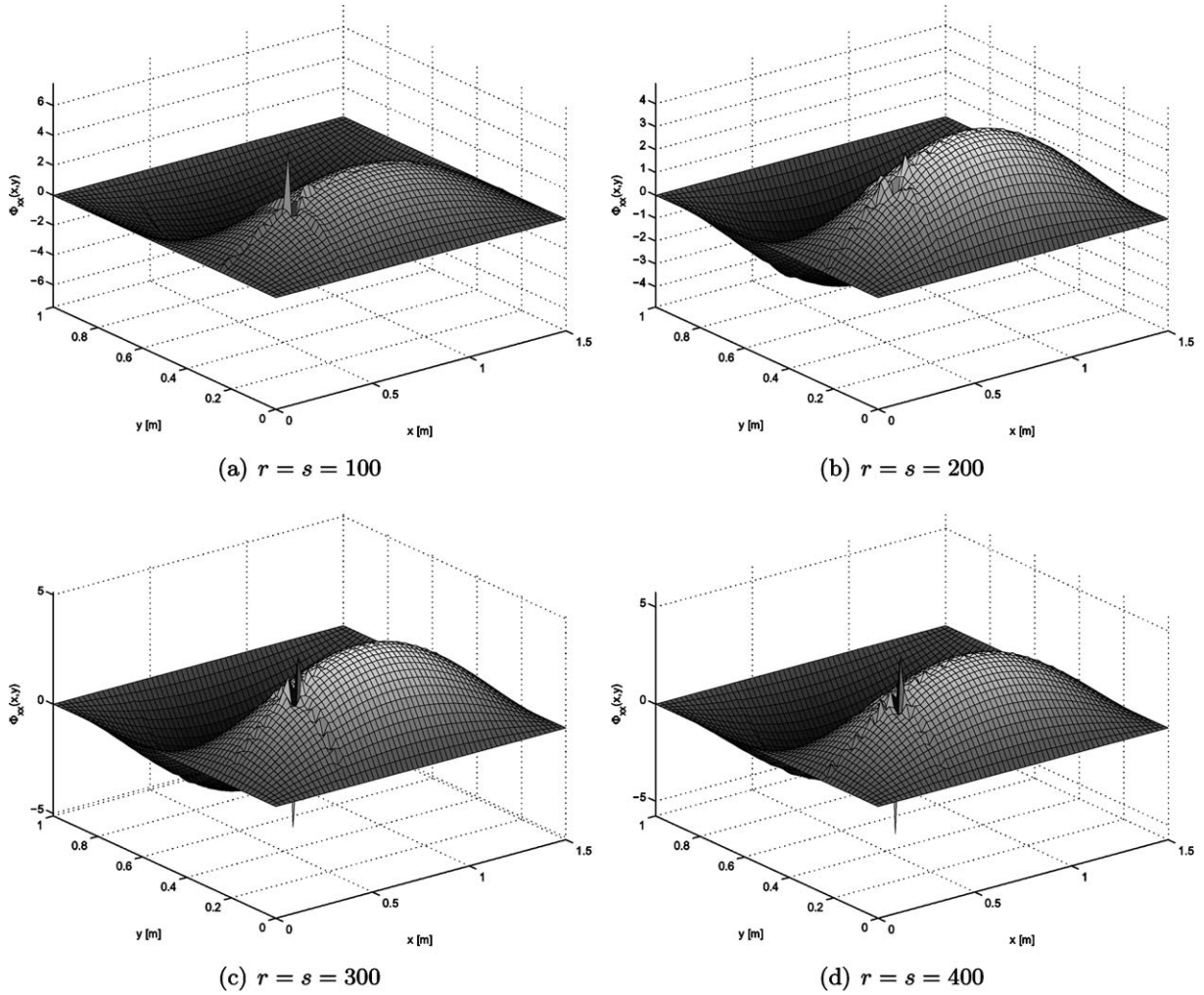

(a) $r = s = 100$ (b) $r = s = 200$

(c) $r = s = 300$ (d) $r = s = 400$

Fig. 3. Curvature $\phi_{12_{xx}}$ estimation using increasing orders of Fourier series expansion.

and

$$\kappa_1 = \frac{4D_0 b_x}{L_x L_y}\left(\left[\left(\frac{i\pi}{L_x}\right)^2 + \left(\frac{j\pi}{L_y}\right)^2\right] - \frac{1}{3}\frac{m_0}{D_0}\lambda^{(0)}\right)\left(\sin\frac{i\pi x_D}{L_x}\right)^2 \int_{y_1}^{y_2}\left(\sin\frac{j\pi\eta}{L_y}\right)^2 d\eta$$

which respectively define the value of κ_1 for a notch damage and for line defects along the x and y directions. Similar expressions, here omitted for the sake of brevity, are obtained for the parameter κ_2.

The amplitude of the Fourier series coefficients $\eta_{r,s}$ can instead by obtained by letting $r \neq i$ and $s \neq j$ in Eq. (22). Summation of the various terms of the Fourier series expansion gives an approximate expression for the first order perturbation eigenvalues and eigenvectors, according to Eqs. (15) and (16).

The results obtained from the formulation presented above are here used to assess the influence of various damage levels, at different locations on the plate surface. Natural frequencies (or eigenvalues),

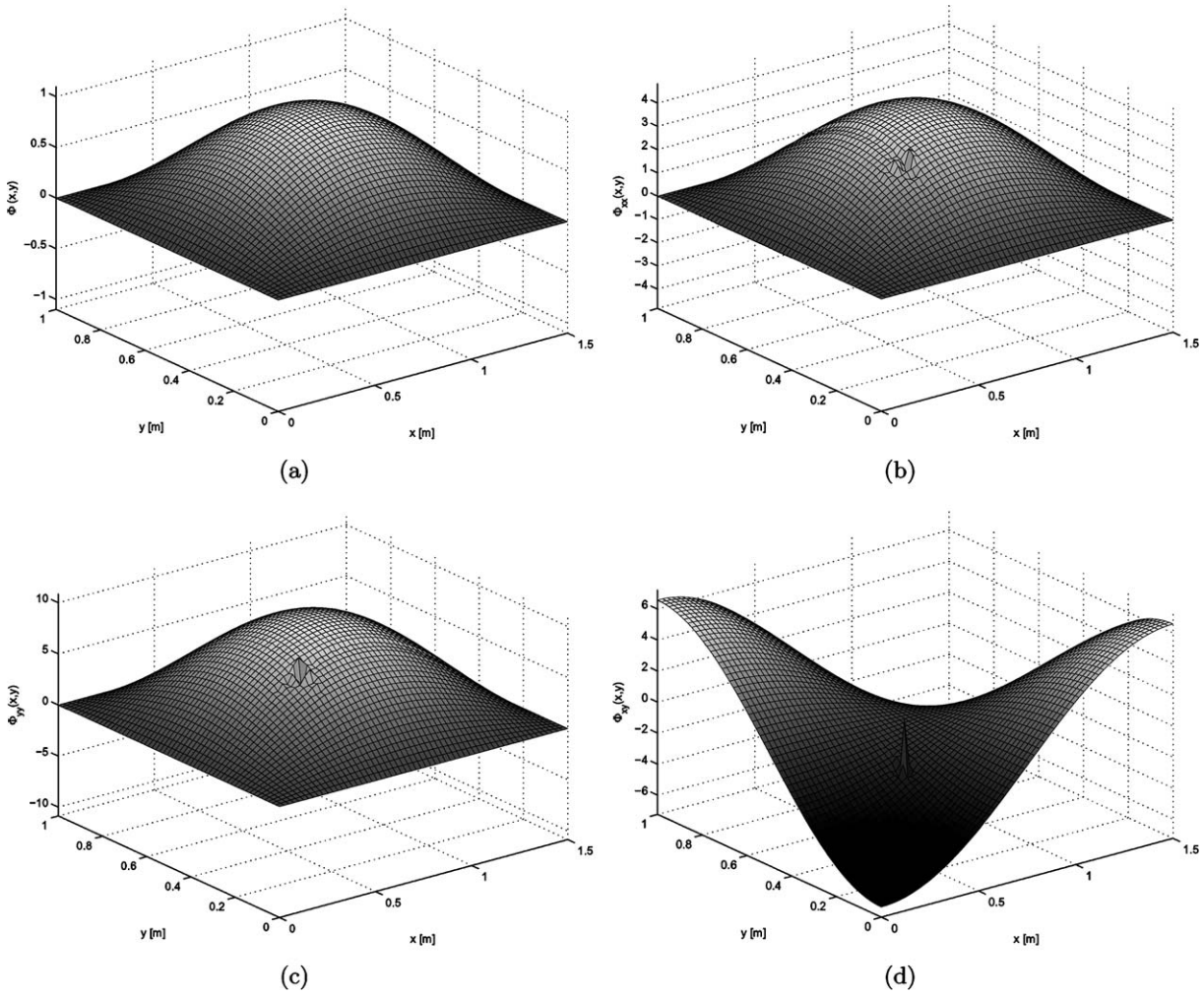

Fig. 4. Deflection and curvatures for mode (1,1) with $h_D/h_0 = 2\%$ and damage located at $x_D = L_x/3$, $y_D = L_y/3$.

modal deflections, as well as modal curvatures are studied as damage indicators to be used in the development of a modal-based damage detection theory. The modal curvatures can be easily computed from the obtained perturbation solution, and they are given by:

$$\begin{aligned}
\phi_{ij,xx} &= -\left(\frac{i\pi}{L_x}\right)^2 \sin\frac{j\pi x}{L_x}\sin\frac{i\pi x}{L_y} - \sum_r\sum_s \eta_{r,s}\left(\frac{r\pi}{L_x}\right)^2 \sin\frac{r\pi x}{L_x}\sin\frac{s\pi x}{L_y} + \mathcal{O}(\epsilon^2)\\
\phi_{ij,yy} &= -\left(\frac{i\pi}{L_y}\right)^2 \sin\frac{i\pi x}{L_x}\sin\frac{j\pi x}{L_y} - \sum_r\sum_s \eta_{r,s}\left(\frac{s\pi}{L_y}\right)^2 \sin\frac{r\pi x}{L_x}\sin\frac{s\pi x}{L_y} + \mathcal{O}(\epsilon^2)\\
\phi_{ij,xy} &= \left(\frac{ij\pi^2}{L_xL_y}\right)\cos\frac{i\pi x}{L_x}\cos\frac{j\pi x}{L_y} + \sum_r\sum_s \eta_{r,s}\frac{rs\pi^2}{L_xL_y}\cos\frac{r\pi x}{L_x}\cos\frac{s\pi x}{L_y} + \mathcal{O}(\epsilon^2)
\end{aligned} \tag{27}$$

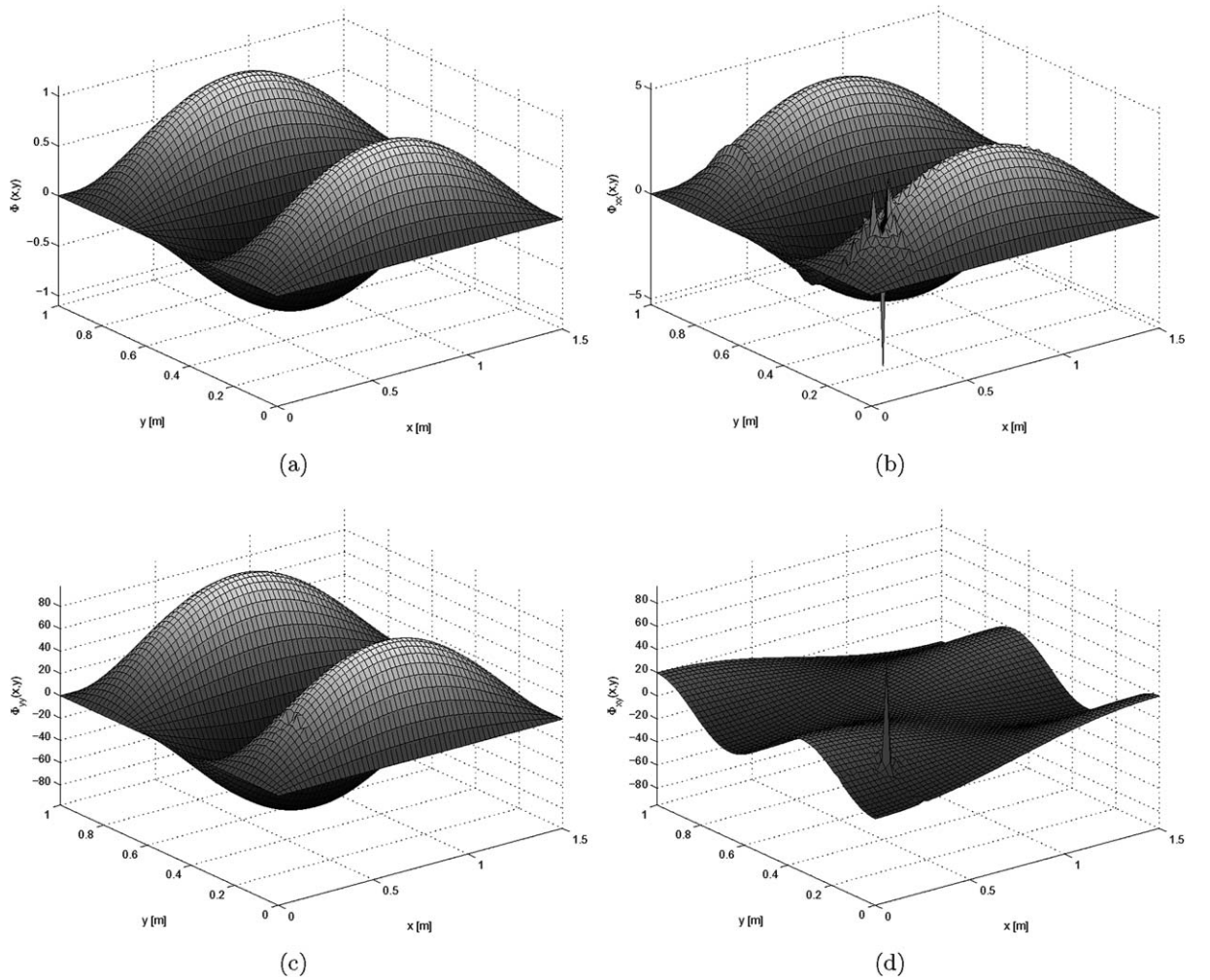

Fig. 5. Mode 1,3: Deflection and curvatures for $h_D/h_0 = 2\%$ and damage located at $x_D = L_x/5$, $y_D = L_y/5$.

2.5. Strain energy ratio for damage localization

The curvature modes evaluated in the previous section can be used directly as damage indicators, and their analytical expressions can be used to evaluate the extent of damage. Alternatively, the curvatures modes can be utilized for the evaluation of the strain energy of the damaged plate. The strain energy for a rectangular plate vibrating according to mode m,n can be expressed as (Leissa, 1993):

$$U_{m,n} = \frac{1}{2} D_0 \int_0^{L_x} \int_0^{L_y} \phi_{mn,xx}^2 + \phi_{mn,yy}^2 + 2v\phi_{mn,xx}\phi_{mn,yy} - 2(1-v)\phi_{mn,xy}^2 \, \mathrm{d}x \, \mathrm{d}y \tag{28}$$

The evaluation of the strain energy for undamaged and damaged plate can be used as an effective strategy for the identification of damage. Furthermore, the location of the defect can be also evaluated through the estimation of the strain energy over limited regions of the plate corresponding to its subdivision into a grid. The strain energy associated to the i,j area of the plate can be expressed as:

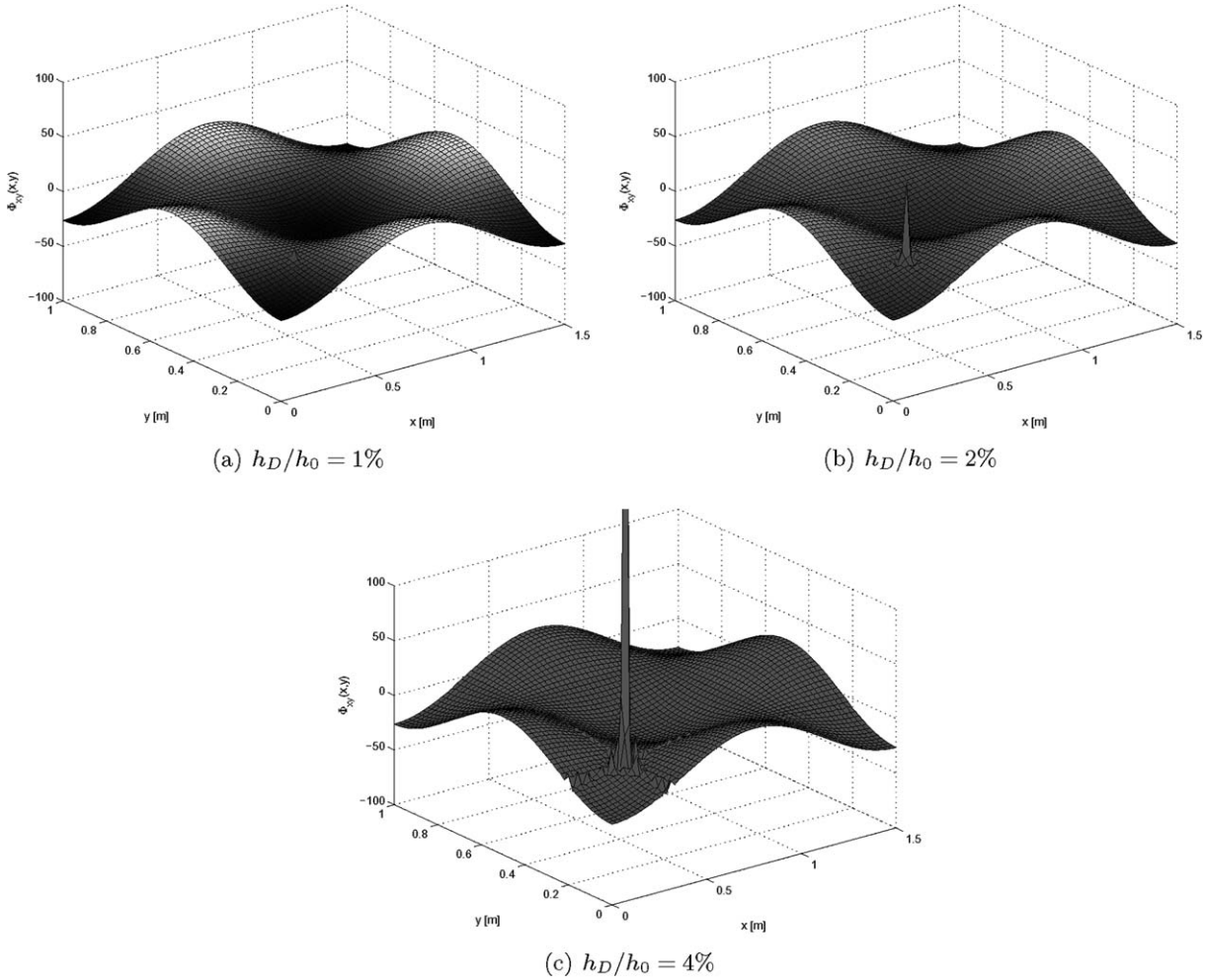

(a) $h_D/h_0 = 1\%$

(b) $h_D/h_0 = 2\%$

(c) $h_D/h_0 = 4\%$

Fig. 6. Influence of increasing damage levels on curvature mode $\phi_{22_{,xy}}$ for notch at $x_D = L_x/5$, $y_D = L_y/5$.

$$U_{m,n}(i,j) = \frac{1}{2} D_0 \int_{x_i}^{x_{i+1}} \int_{y_j}^{y_{j+1}} \phi_{mn,xx}^2 + \phi_{mn,yy}^2 + 2v\phi_{mn,xx}\phi_{mn,yy} - 2(1-v)\phi_{mn,xy}^2 \, dx\, dy \tag{29}$$

We define the modal strain energy ratio (SER) at location i,j as:

$$\sigma_{m,n}(i,j) = \frac{U_{m,n}(i,j)}{U_{m,n}^{(0)}(i,j)} \tag{30}$$

where U, $U^{(0)}$ respectively denote the strain energies of the damage and undamaged plate at the considered location. The strain energy for the damaged plate can be obtained by using the curvatures obtained from the first order perturbation solution. Imposing Eq. (27) in Eq. (32) and neglecting higher powers of ϵ allows expressing the strain energy for the damaged plate as:

$$U_{m,n}(i,j) = U_{m,n}^{(0)}(i,j) - \epsilon \Delta U_{m,n}(i,j) \tag{31}$$

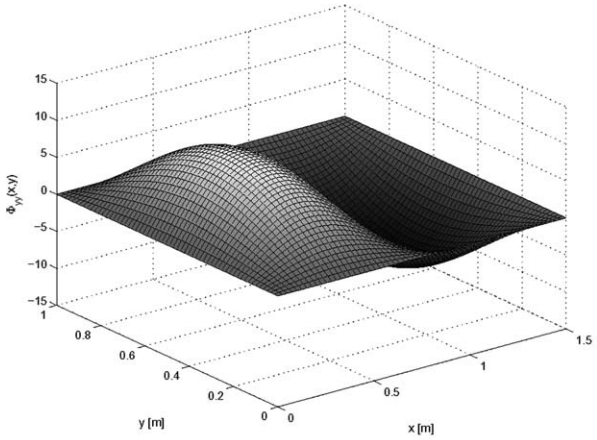

(a) $x_D = L_x/2$, $y_D = L_y/2$

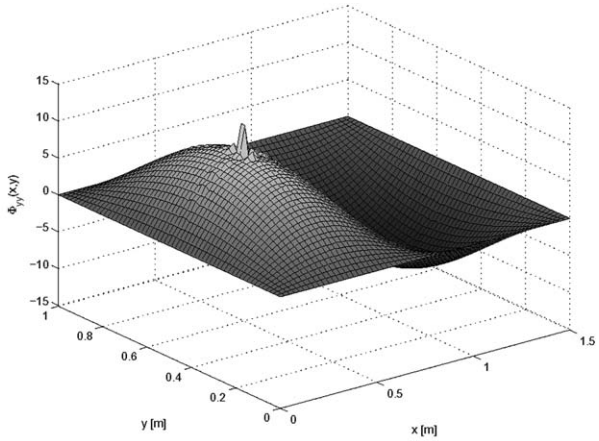

(b) $x_D = L_x/4$, $y_D = L_y/2$

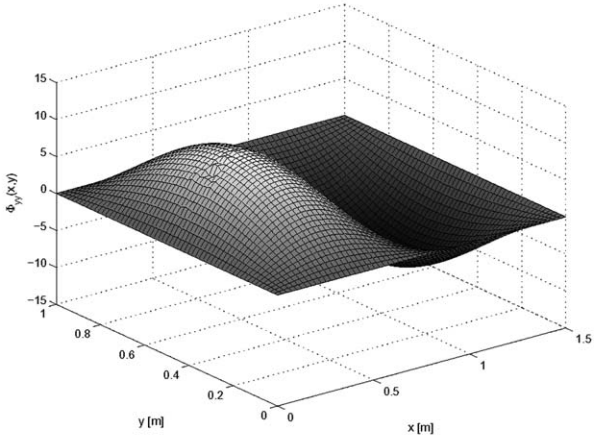

(c) $x_D = L_x/8$, $y_D = L_y/2$

Fig. 7. Influence on damage location on curvature mode $\phi_{21,yy}$ for $h_D/h_0 = 2\%$.

where

$$\Delta U_{m,n}(i,j) = 2D_0 \int_{x_i}^{x_{i+1}} \int_{y_j}^{y_{j+1}} \phi^{(1)}_{mn,xx}\phi^{(0)}_{mn,xx} + \phi^{(1)}_{mn,yy}\phi^{(0)}_{mn,yy} + 2(1-v)\phi^{(1)}_{mn,xy}\phi^{(0)}_{mn,xy} + \frac{1}{2}v\left(\phi^{(1)}_{mn,xx}\phi^{(0)}_{mn,yy} + \phi^{(1)}_{mn,yy}\phi^{(0)}_{mn,xx}\right) \mathrm{d}x\,\mathrm{d}y$$

The SER can be therefore expressed as:

$$\sigma_{m,n}(i,j) = 1 - \epsilon\frac{\Delta U_{m,n}(i,j)}{U^{(0)}_{m,n}(i,j)} \tag{32}$$

The modal SER provides indications regarding the integrity of the area i, j as any variation from unity indicates a difference between the curvature modes over the particular area. A similar concept has been

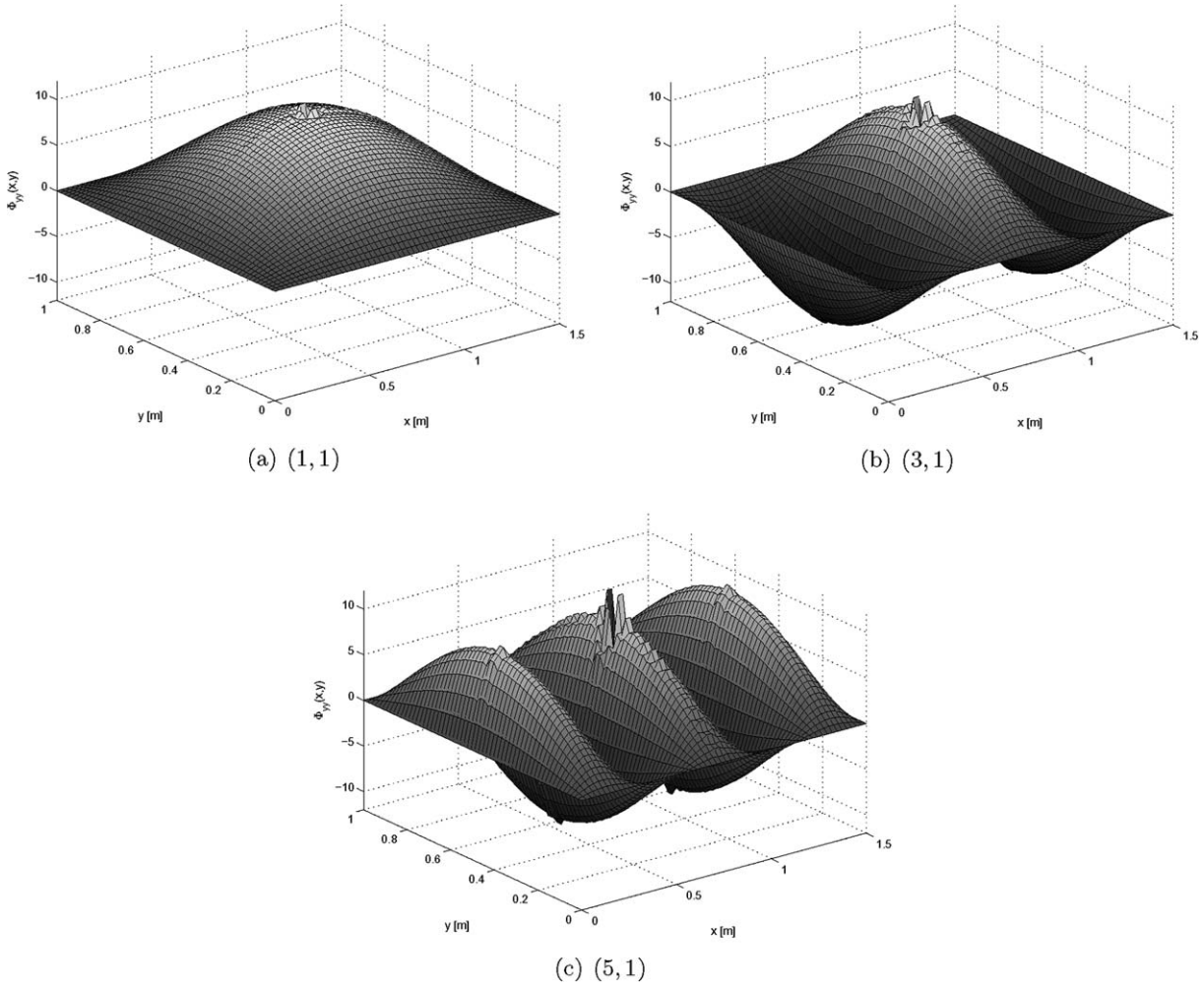

(a) (1,1) (b) (3,1)

(c) (5,1)

Fig. 8. Influence on mode order on curvature mode $\phi_{ij,yy}$ for $h_D/h_0 = 2\%$.

proposed in the literature in Kim and Stubbs (1998) and Hu et al. (1991). The analytical framework of the perturbation analysis of the plate provides a theoretical description of the concept, which, to the best of our knowledge, has never been presented. The presented analytical study also offers the opportunity of quantifying the extent of damage through the value of the SER, which is directly related to the level of damage ϵ.

The definition of strain energy ratio in Eq. (32) considers only one mode of the structure. However it is well known that damage mostly affects regions of higher strain energy. It is thus convenient to sum information obtained from the analysis of several modes m,n and therefore to consider a cumulative strain energy ratio, which may be defined as

$$\sigma(i,j) = \sum_{m,n} \sigma_{m,n}(i,j) = 1 - \epsilon \sum_{m,n} \frac{\Delta U_{m,n}(i,j)}{U^{(0)}_{m,n}(i,j)} \tag{33}$$

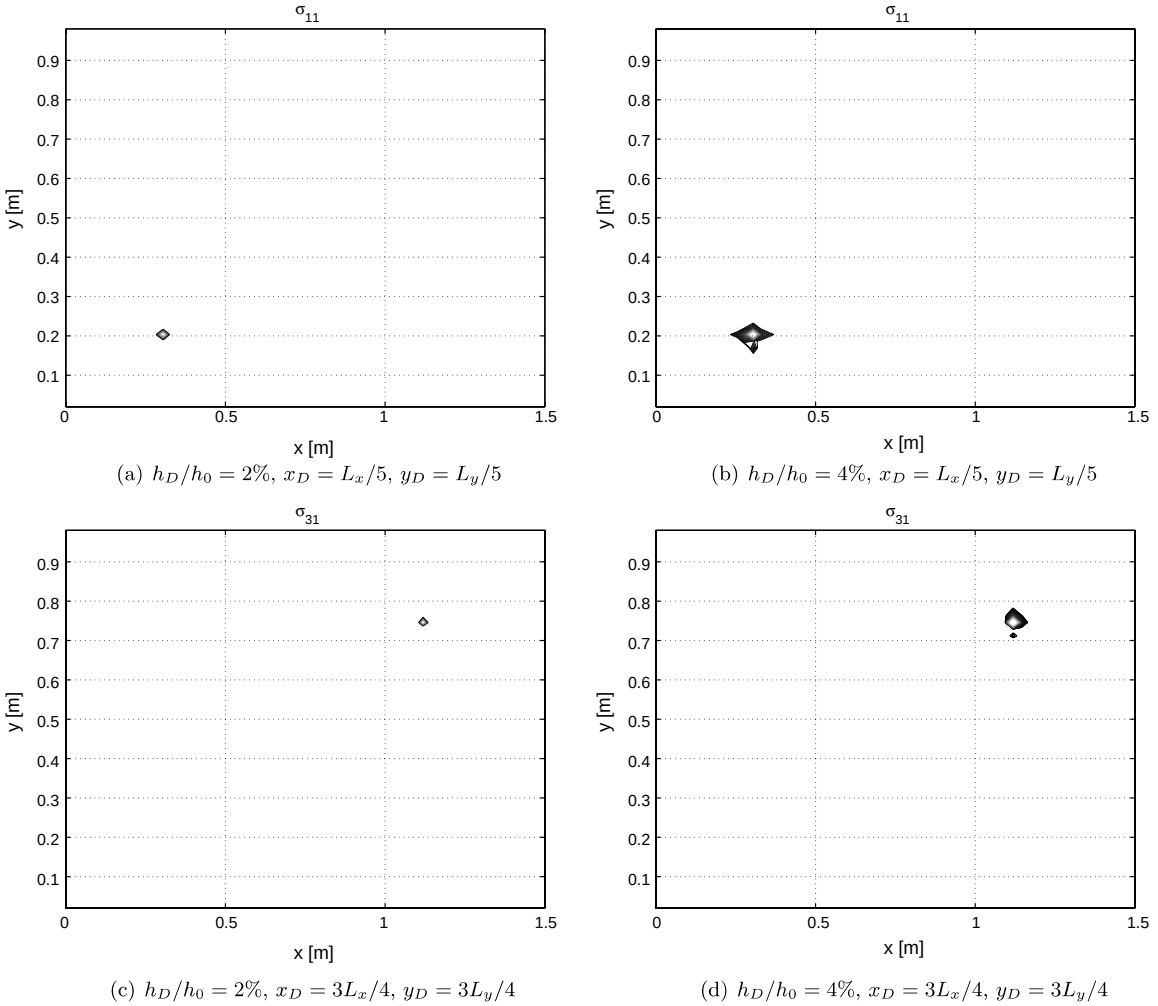

(a) $h_D/h_0 = 2\%$, $x_D = L_x/5$, $y_D = L_y/5$

(b) $h_D/h_0 = 4\%$, $x_D = L_x/5$, $y_D = L_y/5$

(c) $h_D/h_0 = 2\%$, $x_D = 3L_x/4$, $y_D = 3L_y/4$

(d) $h_D/h_0 = 4\%$, $x_D = 3L_x/4$, $y_D = 3L_y/4$

Fig. 9. Examples of modal SER for various damage locations and extents.

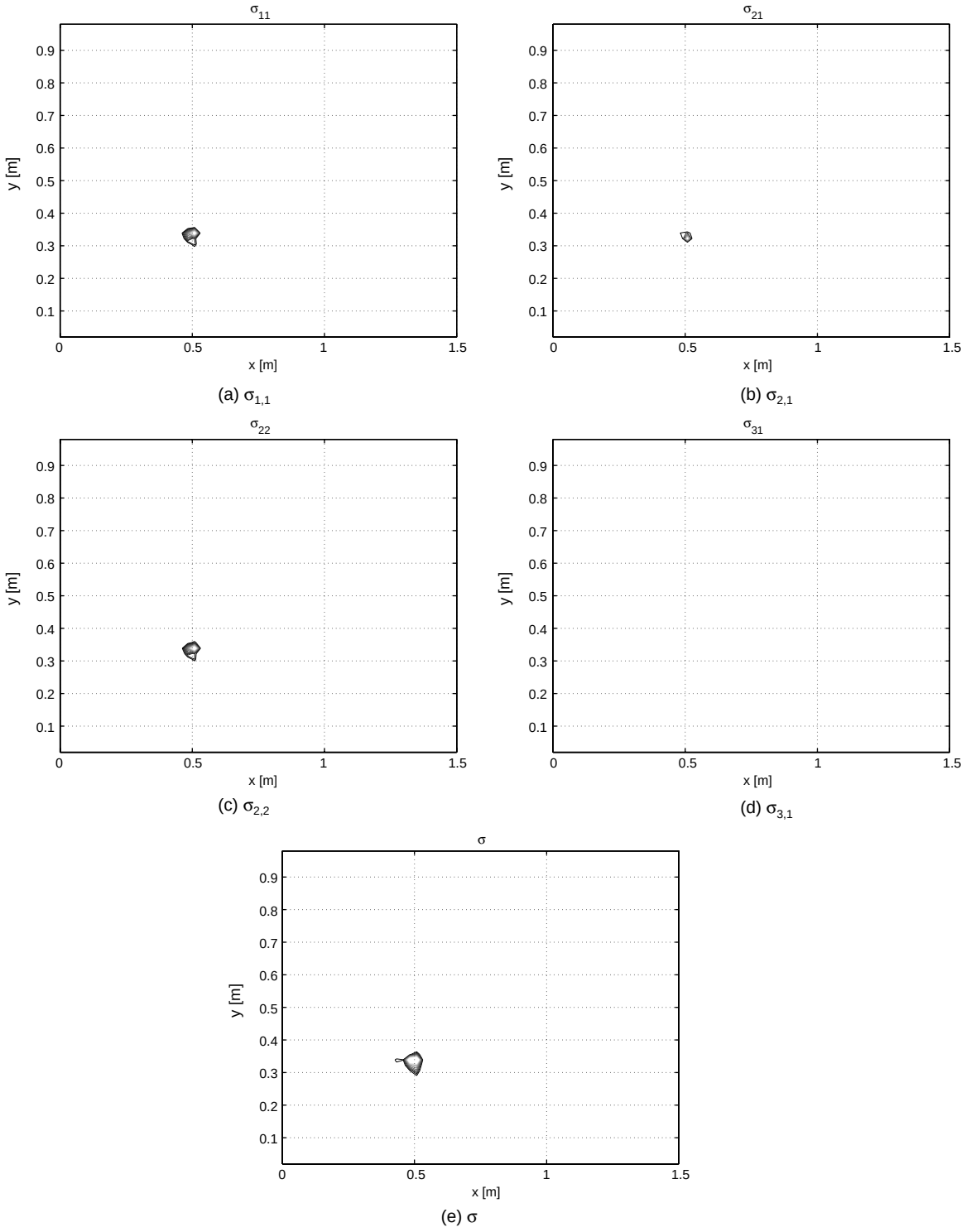

Fig. 10. Modal and cumulative SER for $x_D = L_x/3$, $y_D = L_y/3$ and $h_D/h_0 = 4\%$.

This cumulative index provides a unique information which combines the results from several modes. Modes not affected by damage because of its particular location will not contribute, whereas the index for modes altered by the defect will be combined to provide a robust indication of damage.

3. Results for notch damage

3.1. Plate geometry and material properties

The perturbation analysis presented in the previous section is applied to evaluate natural frequencies, mode shapes and curvature modes of damage plates. Initial results consider the effect of notch damage at various locations, while the investigation of the effects of line defects is presented in the following section. The complete study is performed on a rectangular plate with $L_x = 1.5$ m and $L_y = 1$ m, supported on all

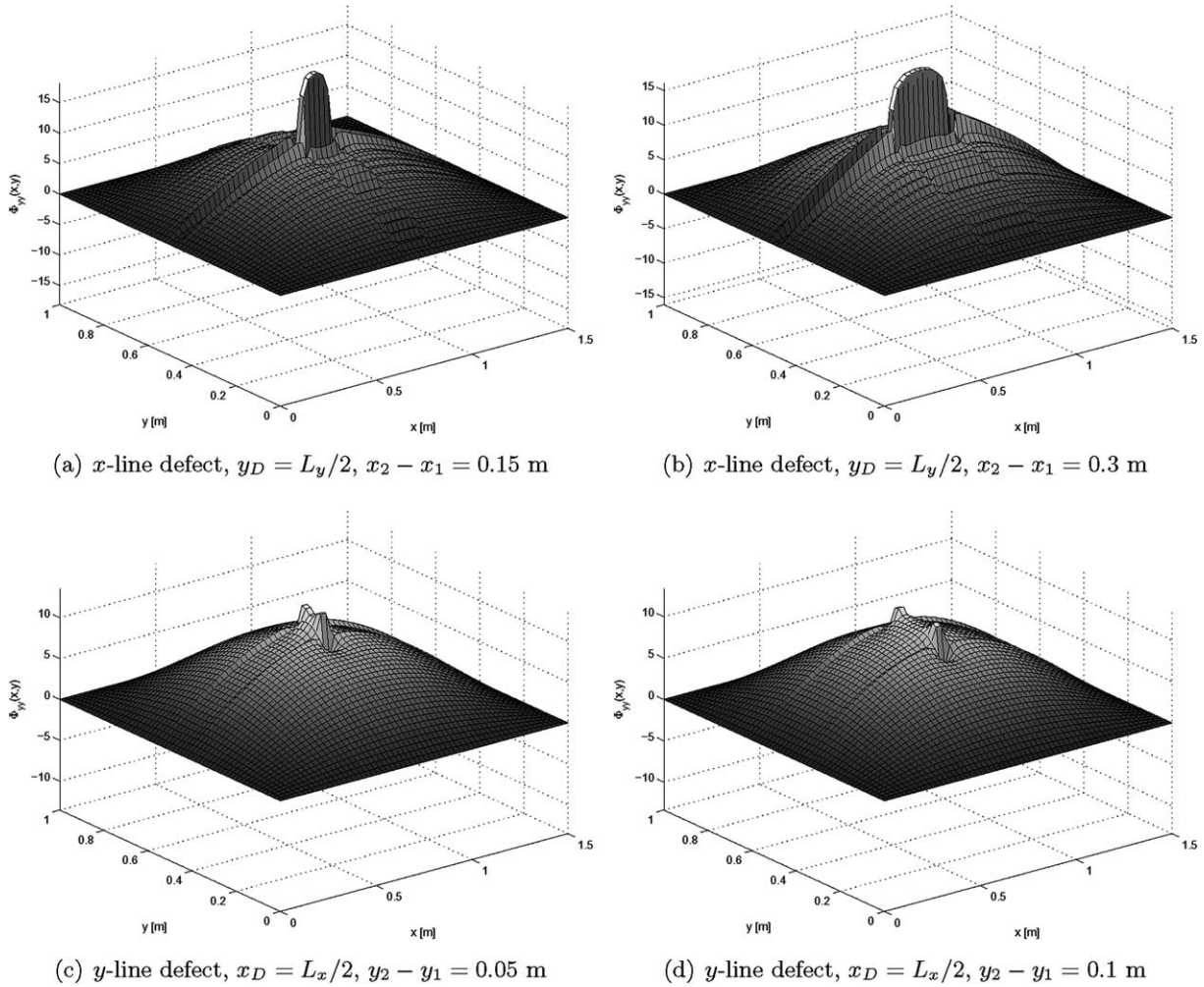

(a) x-line defect, $y_D = L_y/2$, $x_2 - x_1 = 0.15$ m

(b) x-line defect, $y_D = L_y/2$, $x_2 - x_1 = 0.3$ m

(c) y-line defect, $x_D = L_x/2$, $y_2 - y_1 = 0.05$ m

(d) y-line defect, $x_D = L_x/2$, $y_2 - y_1 = 0.1$ m

Fig. 11. Curvature mode $\phi_{11_{yy}}$ for $h_D/h_0 = 4\%$ and line defects of various lengths and orientations.

edges as assumed in the analytical derivations. The plate has a thickness $h_0 = 5$ mm and it is made of aluminum ($E = 7.1 \times 10^{10}$ Pa, $\rho = 2700$ kg/m^3, $\nu = 0.3$). The extent of damage is varied and it is defined by the parameter ϵ according to the definition given in the previous section.

3.2. Natural frequencies

The effect of a notch damage on the plate natural frequencies is first investigated. Various damage locations as well as damage extents are considered for the analysis. The results of the investigations are presented in Table 1. Damage in general tends to reduce the natural frequencies, as a result of the associated stiffness reduction. It is interesting to observe how frequencies remain unchanged when damage is located at the intersection of the nodal lines of the corresponding mode shape as demonstrated by the frequency of mode (2,2) for damage at $x_D = L_x/2$, $y_D = L_y/2$. Also frequencies corresponding to higher order modes

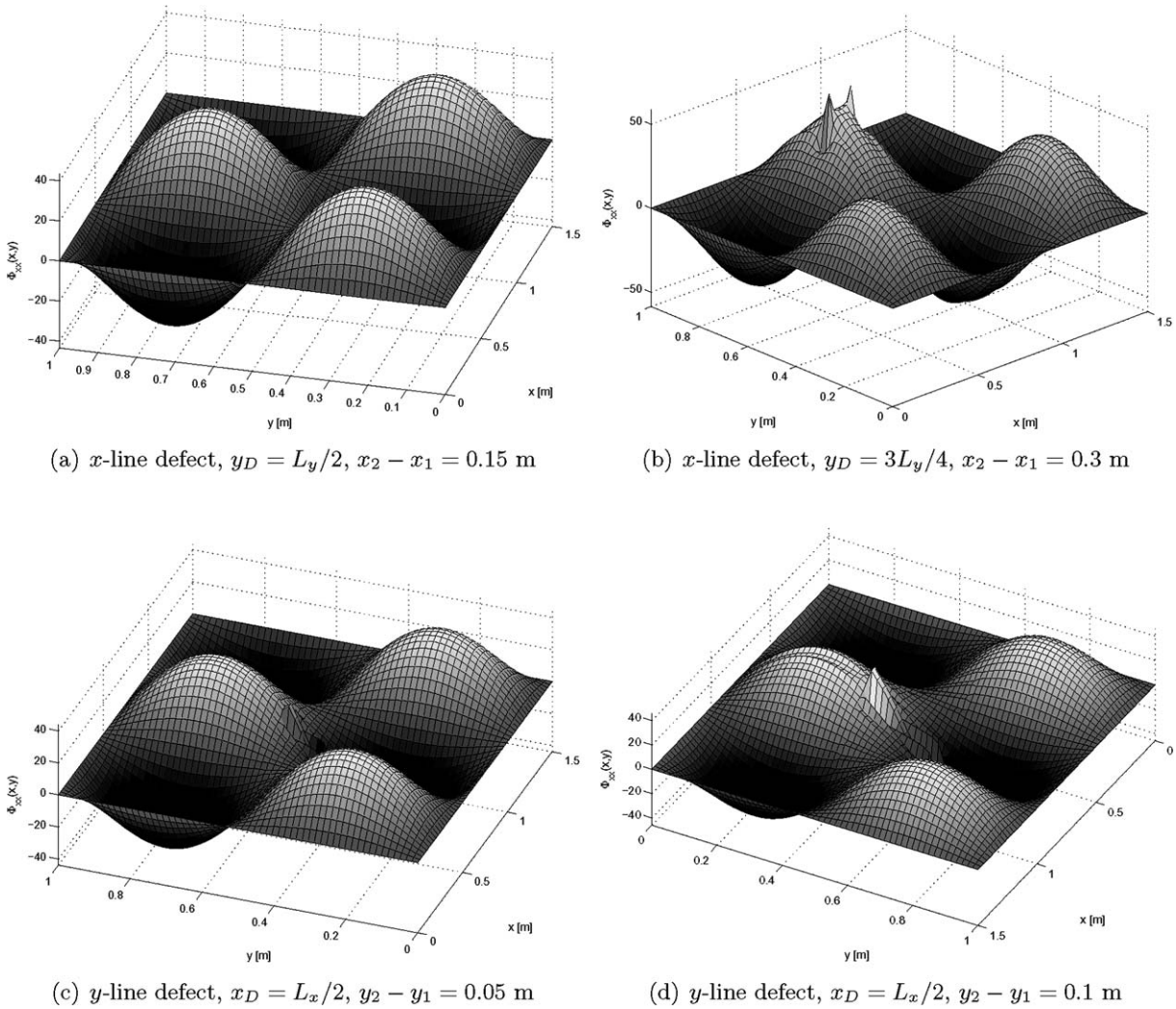

(a) x-line defect, $y_D = L_y/2$, $x_2 - x_1 = 0.15$ m

(b) x-line defect, $y_D = 3L_y/4$, $x_2 - x_1 = 0.3$ m

(c) y-line defect, $x_D = L_x/2$, $y_2 - y_1 = 0.05$ m

(d) y-line defect, $x_D = L_x/2$, $y_2 - y_1 = 0.1$ m

Fig. 12. Curvature mode $\phi_{32_{xx}}$ for $h_D/h_0 = 4\%$ and line defects of various lengths, locations and orientations.

tend to be more affected by the presence of damage, as demonstrated for example by the comparison of the frequency changes in modes (1, 1) and (1, 3).

3.3. Modal deflections and curvatures

Modal deflections and curvatures for plates with notch damage are evaluated through the procedure presented above. The perturbation analysis is limited to the first order based on previous results for beams, which have shown how the second order term gives minor contributions (Luo and Hanagud, 1998). The Fourier series expansions are performed by considering the superposition of 300 terms. This number has been selected after the qualitative analysis of mode shapes and curvatures predicted with increasing number of expansion terms. A sample of these investigations is shown in Fig. 3, which presents the curvature $\phi_{ij,xx}$ for mode (1, 2) estimated with increasing number of terms in the expansion. In the plot, the presence of

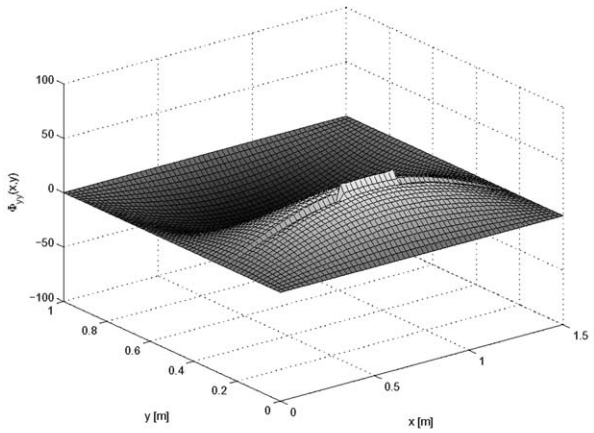

(a) x-line defect, $y_D = L_y/4$, $x_2 - x_1 = 0.3$ m, $h_D/h_0 = 2\%$

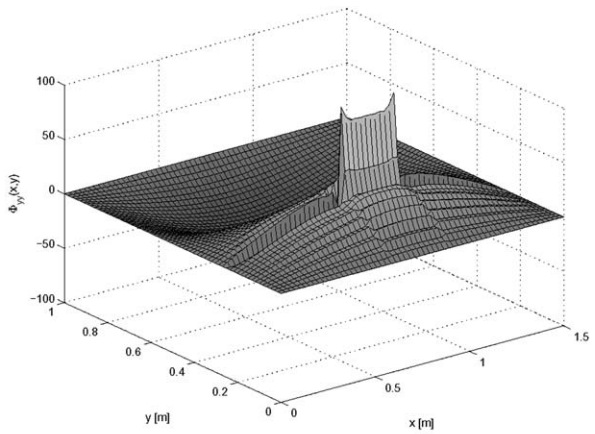

(b) x-line defect, $y_D = L_y/4$, $x_2 - x_1 = 0.3$ m, $h_D/h_0 = 4\%$

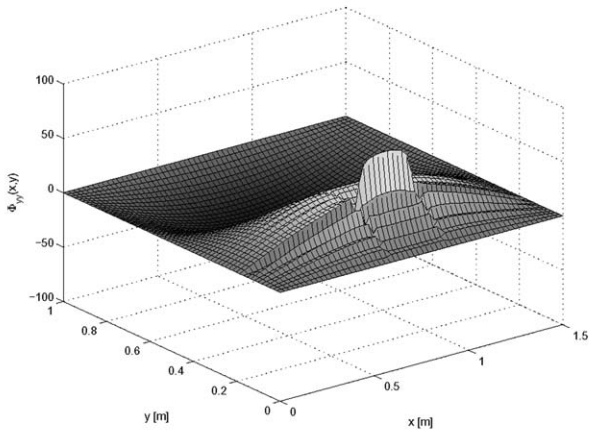

(c) x-line defect, $y_D = L_y/6$, $x_2 - x_1 = 0.3$ m, $h_D/h_0 = 4\%$

Fig. 13. Influence of extent and location of damage on curvature mode $\phi_{12,yy}$.

damage is demonstrated by a peak at the corresponding location. It is easy to observe how 300 terms are able to fully capture the peak and that considering higher numbers of terms does not provide additional details on damage. Series expansion with 300 terms are therefore used in our study as a good compromise between accuracy and computational efficiency. Examples of modal deflections and curvatures are shown in Figs. 4–8 for several combinations of damage location and damage extent. The results for modes (1, 1) and (1, 3) are presented in Figs. 4 and 5, which clearly demonstrate how for the considered level of damage, the deflection mode shapes are not affected by the presence of the notch, while the curvature modes highlight its presence through a peak at the corresponding locations. The amplitude of the peak is proportional to the extent of damage as shown in Fig. 6, which depicts the curvature mode $\phi_{22_{xy}}$ for increasing damage ratios h_D/h_0. The effect of damage on the curvature modes also depends on its location with respect to the nodal lines of the corresponding mode shapes. Fig. 7 shows for example how a notch damage with $h_D/h_0 = 2\%$ becomes more evident when it is located close, or at the points of maximum curvature. Finally, Fig. 8

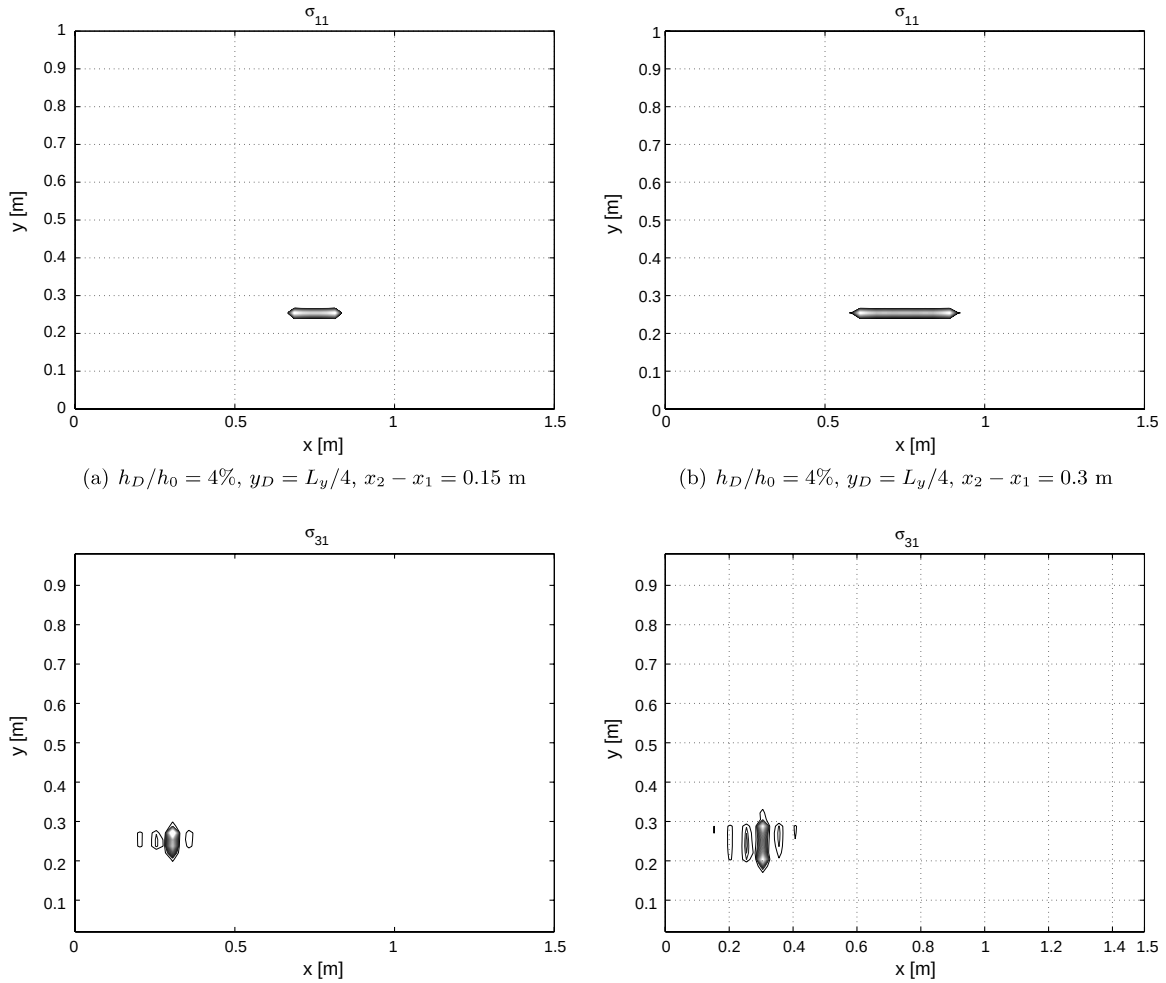

(a) $h_D/h_0 = 4\%$, $y_D = L_y/4$, $x_2 - x_1 = 0.15$ m

(b) $h_D/h_0 = 4\%$, $y_D = L_y/4$, $x_2 - x_1 = 0.3$ m

(c) $h_D/h_0 = 4\%$, $y_2 - y_1 = 0.05$ m, $x_D = L_x/5$

(d) $h_D/h_0 = 4\%$, $y_2 - y_1 = 0.1$ m, $x_D = L_x/5$

Fig. 14. Examples of modal SER for various damage locations and extents.

compares the effects of a defect of assigned extent on various modes, and demonstrates how the notch tends to affect more significantly higher order modes than lower order modes. This observation confirms the remarks made regarding the natural frequencies of the damaged plates listed in Table 1.

3.4. Strain energy ratio for damage localization

The strain energy ratio (SER) defined in the previous section is here used for the estimation of damage location and extent. The SER is computed by discretizing the plate surface into a 60×60 grid, over which the strain energy and its variation with respect to the undamaged configuration are computed. The integration required for the SER evaluation are evaluated analytically, due the convenient formulation for the undamaged and damaged curvature modes obtained through the perturbation analysis. Results for notch defects are presented in Figs. 9 and 10, where the SER distributions are represented as contour plots. The abscissa and ordinates respectively represent the plate length L_x and width L_y, while the magnitude of the SER is indicated by a gray color scale varying between a minimum of 1.05 (black) to a maximum of 2 (white). The presence of the defect in the presented maps is highlighted by a peak at the corresponding location, which stands out very evidently on the white background imposed on the figure. The extent of the peak and mostly its magnitude are proportional to the damage extent and specifically to the parameter ϵ or to the ratio h_D/h_0 as predicted by Eqs. (32) and (33). The correlation between damage extent and magnitude of the SER is shown in Fig. 9, which presents modal SER results for notch defects of different extent and location. The application of the superposition of modal SER distributions to obtain a single damage index is instead illustrated in Fig. 10, which shows modal SER values for an assigned damage configuration and the result of the combinations of the modal contributions according to Eq. (33). As discussed above, various modes have in fact different sensitivity to damage at a specific location. In here for example, it is clear how the considered damage has very little effect on mode (3, 1), as demonstrated by the corresponding modal SER map shown in Fig. 10d. The combination of the various modal contributions however is able to capture the presence of the defect by combining the information provided by each mode.

4. Results for line defects

The presented analytical procedure is also applied to the analysis of line defects of the kind depicted in Fig. 2. Results for various defect lengths, extensions and orientation are presented in Figs. 11–13. Fig. 11 for example shows the influence of damage on the curvature mode $\phi_{11_{,yy}}$. Different defects lengths and orientations are considered to demonstrate how the considered curvature mode highlights the presence of damage through an evident discontinuity at the damage location. The length and the orientation of the discontinuity correspond to those of the considered defect. Fig. 12 presents results for the curvature mode $\phi_{32_{,xx}}$ of a damage plate. The plot in Fig. 12a is obtained for the defect located along the nodal line of the curvature mode and therefore no discontinuity can be observed. The same damage at a different location however becomes clearly evident as shown in the case presented in Fig. 12b. Morever, Fig. 12b and c compare damage discontinuities corresponding to damage of increasing lengths to demonstrate the increased sensitivity of the curvature modes. In Fig. 13 finally, the influence of damage location and extent is demonstrated for mode $\phi_{12_{,yy}}$.

Strain energy ratios are computed also for line defects. Examples of the results are shown in Figs. 14 and 15. The maps presented in Fig. 14 clearly demonstrate how the SER representation is able to provide information regarding damage extent, length and location. Finally, Fig. 15 presents the result of the summation procedure for various modal SER, to obtain a cumulative ratio to be used as a damage index in damage identification routines.

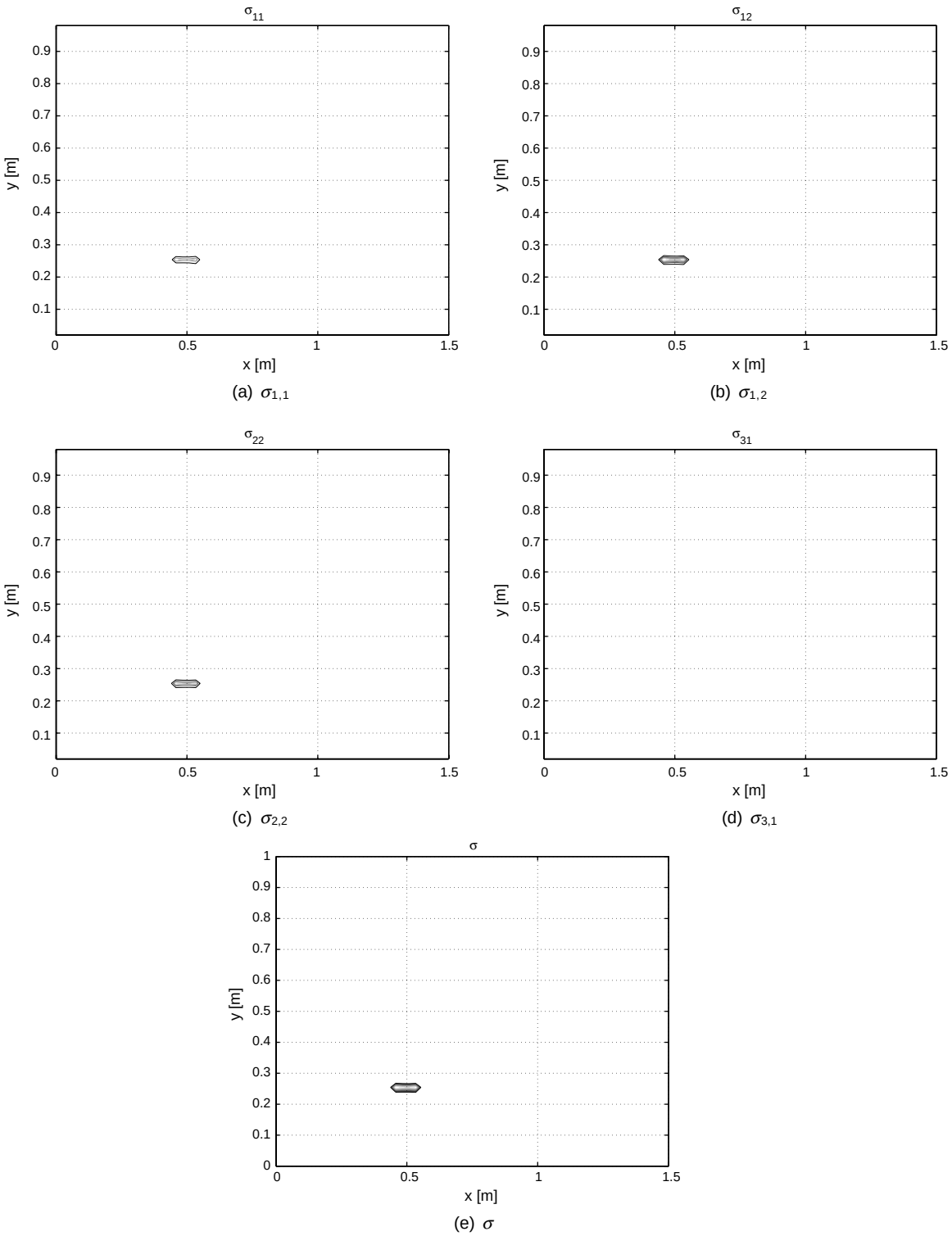

Fig. 15. Modal and cumulative SER for line defect with $x_2 - x_1 = 0.15$ m, $y_D = L_y/4$ and $h_D/h_0 = 2\%$.

5. Experimental evaluation of the strain energy ratio

The application of the developed concept for the analysis of experimentally measured curvature modes is presented in this section. The presented results demonstrate the effectiveness of SER as a damage indicator, and show how it can be practically implemented as part of an inspection technique for plate-like structures. The results in this section cannot be directly compared with those obtained analytically, as boundary conditions and damage orientation are different than those considered in the previous analysis. However, we here outline the procedure for carrying out the SER analysis based on experimental measurements and we show that damage can be correctly identified using the developed procedure. A detailed description of the experimental procedure and a complete set of results are presented in a companion paper by the same authors (Sharma et al., 2005).

5.1. Experimental set-up

The considered test specimen is an aluminum plate of dimensions 14 in. × 14 in. × 0.040 in. The plate is cantilevered at its base. A piezoceramic disc of 1.1 in. diameter and 0.030 in. thickness is used as an exciter. The placement of the actuator is selected in order to excite the highest number of modes of the structure. Plate, with actuator and damage location is shown in Fig. 16a. The actuator was simply bonded to the plate using a Loctite Quick Set epoxy. The disc was also fully encased in a layer of epoxy to provide it with an adequate backing to impart sufficient force to its base. A set of simple tests were conducted to ensure that the effectiveness of the actuator in exciting the vibration modes and to check for durability of the bonding epoxy, which demonstrated to be excellent. The damage is a 1.41 in. long, 0.05 in. wide and 0.015 deep groove which was cut in the plate at the location shown in Fig. 16a. The plate response was measured using a Scanning Laser Doppler Vibrometer (SLDV) by Polytec PI (model PSV400M2). The SLDV measures the plate vibration at a large number of locations, thus providing unprecedented amount of information. The measurement grid used for the tests is shown in Fig. 16b. The responses at the grid points is recorded, stored, and converted into Matlab® for post-processing. In particular, the responses are interpolated using spline functions, which can be conveniently differentiated for curvature evaluation. The process of

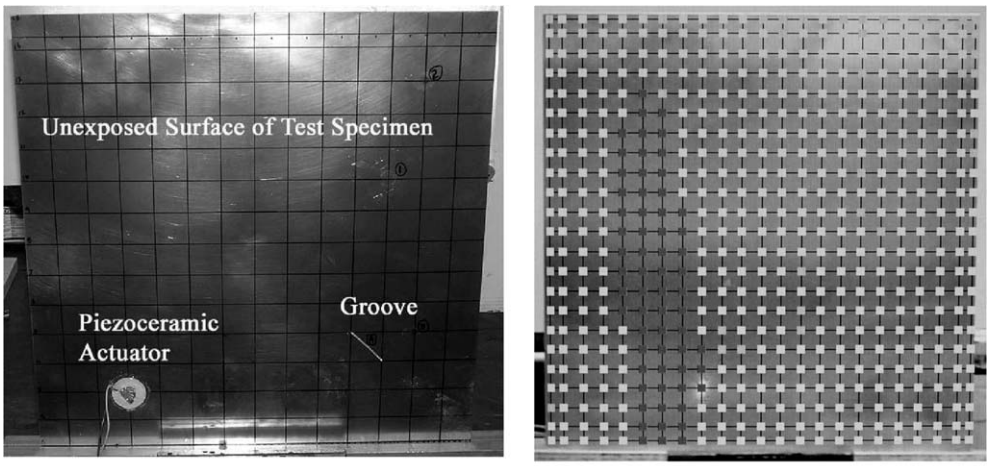

(a) Aluminum plate used for SER tests (b) Measurement grid

Fig. 16. Cantilevered aluminum plate with detail of actuator and damage locations (a), and measurement grid (b).

interpolation using splines minimizes the numerical errors associated with the spatial differentiation and reduces the influence of noise in the data, as the differentiation is performed on the spline functions, while the measured data simply act as weighting parameters for the interpolation of response and corresponding curvatures (Sharma et al., 2005).

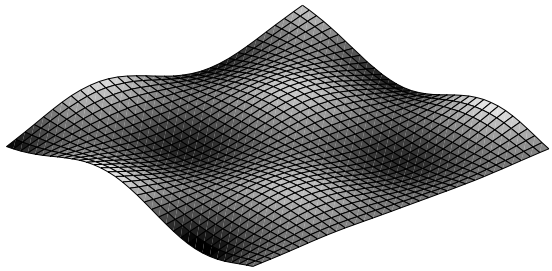

(a) ODS at 270 Hz

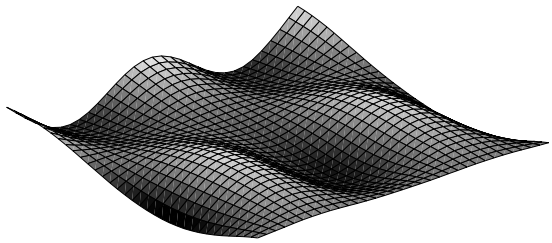

(b) ODS at 293 Hz

Fig. 17. Examples of experimentally measured ODS.

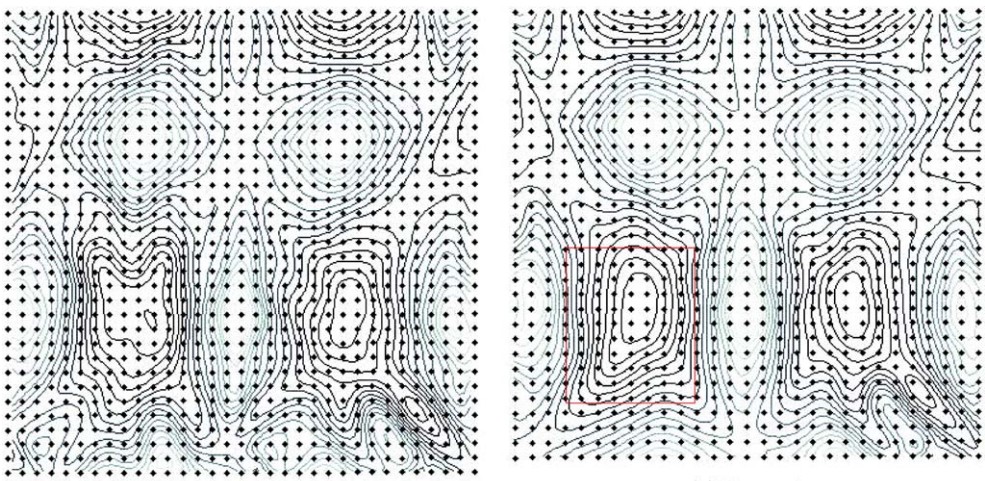

(a) Undamaged (b) Damaged

Fig. 18. Curvature at 180 Hz for undamaged and damaged plate.

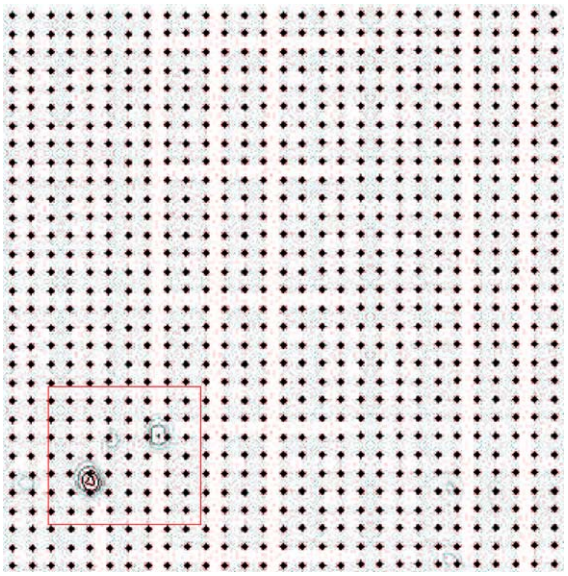

Fig. 19. Experimentally evaluated SER through the superposition of first 5 modes.

5.2. Results

The plate is excited in the 0–500 Hz range using pseudo-random excitation. The forced response at the plate natural frequencies, often denoted as Operational Deflection Shape (ODS), and corresponding curvatures in the excitation range are evaluated. Fig. 17 shows for example the measured ODS at 270 and 293 Hz, while Fig. 18 compares the curvature at 182 Hz for the undamaged and damaged plate. The two curvatures show differences at the damage location and their comparison can be used for the assessment of the presence of the groove. A more definite indication is however provided by the SER map presented in Fig. 19, which clearly shows a deviation from unity at the damage location. The SER is obtained using the interpolated curvatures for damaged and undamaged plate and is the superposition of the first 5 measured modes.

6. Conclusions

The dynamic behavior of damaged plates is investigated through perturbation techniques. This analytical framework allows investigating the effect of various types of damage on the plate modal parameters and the formulation of a strain energy ratio index which can be used for damage identification purposes. The formulation considers both point damage, as well as line defects which can be considered as simple descriptions of longitudinal cracks or delaminations. Variation of natural frequencies, mode shapes and curvature modes are investigated for the considered types of defects. The results indicate the high sensitivity of curvature modes even in the presence of low levels of damage. These investigations therefore confirm results previously obtained for beam structures and suggest the possible application of curvature modes as efficient damage indicators. In addition, the curvature modes are used for the estimation of the plate strain energy and to formulate a Strain Energy Ratio, which can be used to effectively identify location as well as the extent of the defects. The presented analytical results provide invaluable insights on the effect of damage on the plate modal parameters, and are used in support of experimental activities aimed at

relating curvature changes in plate structures to the level and location of defects. An example of the results obtained experimentally on plate structures is also presented in the final section of the paper.

Acknowledgement

The authors acknowledge the support of the Air Force Office of Scientific Research (AFOSR), which provided funding for this work under the contract No. FA9550-04-C-0116 monitored by Capt. Clark Allred.

References

Atluri, S.N., 1986. Computational Methods In The Mechanics of Fracture. North Holland, Amsterdam.

Azak, A., Krawczuk, M., Ostachowicz, W., 2001. Vibration of a laminated composite plate with closing delamination. Journal of Intelligent Material Systems and Structures 12 (8), 545–551.

Christides, S., Barr, A.D.S., 1984. One-dimensional theory of cracked Euler–Bernoulli beams. International Journal of Mechanical Sciences 26 (11–12), 639–648.

Doebling, S.W., Farrar, C., Prime, M.B., Daniel, W.S., 1996. Damage Identification and Health Monitoring of Structural and Mechanical Systems from Changes in their Vibration Characteristics: A Literature Review, LA-13070-MS, May 1996.

Gudmundson, P., 1984. The dynamic behavior of slender structures with cross-sectional cracks. Journal of Mechanics, Physics and Solids 31, 329–345.

Haisty, B.S., Springer, W.T., 1988. A general beam element for use in damage assessment of complex structures. ASME Journal of Vibration, Acoustics, Stress, and Reliability in Design 110, 356–359.

Hellan, K., 1984. Introduction to Fracture Mechanics. McGraw-Hill, New York.

Hu, N. et al., 1991. Damage assessment of structures using modal test data. International Journal of Solids and Structures 38, 3111–3126.

Jones, D.S., 1982. The Theory of Generalized Functions. Cambridge University Press, Cambridge UK.

Kim, J.T., Stubbs, N., 1998. Crack detection in beam type structures using frequency data. Journal of Sound and Vibration 259 (1), 146–160.

Krawczuk, M., 2002a. Application of spectral beam finite element with a crack and iterative search technique for damage detection. Finite Elements in Analysis and Design 38 (6), 537–548.

Krawczuk, M., 2002b. A rectangular plate finite element with an open crack. Computers and Structures.

Krawczuk, M., Palacz, M., Ostachowicz, W., 2004. Wave propagation in plate structures for crack detection. Finite Elements in Analysis and Design 40 (9–10), 991–1004.

Krawczuk, M., Ostachowicz, W., 1995. Modelling and vibration analysis of a cantilever composite beam with a transverse open crack. Journal of Sound and Vibration 183 (1), 69–89.

Krawczuk, M., Ostachowicz, W., 2002. Identification of delamination in composite beams by genetic algorithm. Science and Engineering of Composite Materials 10 (2), 147–155.

Leissa, A., 1993. Vibration of Plates. Acoustical Society of America, Washington, DC.

Lestari, W., 2001. Damage of Composite Structures: Detection Technique, Dynamic Response and Residual Strength, PhD Thesis, Georgia Institute of Technology.

Luo, H., Hanagud, S., 1998. An integral equation for changes in the structural characteristics of damaged structures. International Journal of Solids and Structures 34 (35–36), 4557–4579.

Ostachowicz, W., Krawczuk, M., 1990. Analysis of the effect of cracks on the natural frequencies of a cantilever beam. Journal of Sound and Vibration 138, 115–134.

Qian, G.L., Gu, S.N., Jiang, J.S., 1991. The dynamic behavior AN crack detection of a beam with a crack. Journal of Sound and Vibration 138, 233–243.

Sharma, V.K., Ruzzene, M., Hanagud, S., 2005. Damage Index Estimation in Beams and Plates Using Laser Vibrometry. AIAA Journal, submitted for publication.

Shen, M.H., Pierre, C., 1990. Natural modes of Euler–Bernoulli beams with symmetric cracks. Journal of Sound and Vibration 138, 115–134.

Staszewski, W.J., Boller, C., Tomlinson, G., 2004. Health Monitoring of Aerospace Structures. Smart Sensors and Signal Processing. Wiley & Sons Ltd.